

# Communication

## Formation of Delta Ferrite in 9 Wt Pct Cr Steel Investigated by *In-Situ* X-Ray Diffraction Using Synchrotron Radiation

P. MAYR, T.A. PALMER, J.W. ELMER, E.D. SPECHT, and S.M. ALLEN

*In-situ* X-ray diffraction (XRD) measurements using high energy synchrotron radiation were performed to monitor in real time the formation of delta ferrite in a martensitic 9 wt pct chromium steel under simulated weld thermal cycles. Volume fractions of martensite, austenite, and delta ferrite were measured as a function of temperature at a 10 K/s heating rate to 1573 K (1300 °C) and subsequent cooling. At the peak temperature, the delta ferrite concentration rose to 19 pct, of which 17 pct transformed back to austenite on subsequent cooling.

DOI: 10.1007/s11661-010-0371-7

© The Author(s) 2010. This article is published with open access at Springerlink.com

Cast martensitic 9 to 12 wt pct chromium steels are widely used for thick-walled high-temperature turbine casings or steam valves in thermal power generation. The chemical composition is carefully balanced between austenite ( $\gamma$ ) stabilizing elements (C, Mn, Ni, Co, Cu, and N) and ferrite ( $\alpha$ ) stabilizers (Si, Cr, W, Mo, V, and Nb) to avoid the presence of stable delta ferrite ( $\delta$ ) at room temperature and the accompanying reduced toughness and ductility.<sup>[1]</sup>

After welding,  $\delta$ -ferrite is often retained in the heat-affected zone of the base material adjacent to the weld fusion line.<sup>[3]</sup> This region is exposed to peak temperatures just below the melting temperature for prolonged periods, promoting the formation of high-temperature phases. Little is known about the formation of  $\delta$ -ferrite, its phase fraction evolution during weld thermal cycles, and the mechanism of retention in a former  $\delta$ -ferrite free

martensitic steel. In this investigation, the formation and dissolution of  $\delta$ -ferrite in a 9 wt pct chromium steel is monitored using *in-situ* X-ray diffraction (XRD) with synchrotron radiation during exposure to a single-weld thermal cycle. These results are then analyzed using thermodynamic equilibrium calculations, dilatometry, metallography, and optical phase fraction analysis.

A 100-kg ingot of an experimental Fe-0.168C-0.23Si-0.22Mn-8.85Cr-1.54Mo-0.18Ni-0.29V-0.057Nb-0.009B-0.016N steel (wt pct) was produced by conventional sand casting. It was normalized at 1373 K (1100 °C) for 8 hours and, after air cooling to room temperature tempered at 1003 K (730 °C) for 10 hours, allowed to air cool to room temperature, and tempered again for an additional 24 hours at this same temperature. A tempered martensite microstructure with no delta ferrite was observed. Finely dispersed precipitates were identified by analytical transmission electron microscopy as Cr-rich  $M_{23}C_6$  carbides, V-rich MX nitrides, and Nb-rich MX carbides.

An equilibrium phase diagram (Figure 1) was calculated using Matcalc<sup>[4]</sup> with the MC\_steel database.<sup>[5]</sup> At the nominal Cr content (8.85 wt pct), equilibrium phase transformation temperatures are predicted at  $A_{e1} = 1113$  K (840 °C),  $A_{e3} = 1168$  K (895 °C), and  $A_{e4} = 1497$  K (1224 °C), where  $A_{e1}$  indicates the onset of austenite formation,  $A_{e3}$  the achievement of a fully austenitic state, and  $A_{e4}$  the start of  $\delta$ -ferrite formation on heating. During cooling, the steel passes through the single-phase austenite ( $\gamma$ ) region and a fully martensitic microstructure with no stable  $\delta$ -ferrite at room temperature is formed after it passes through the martensite start temperature ( $M_S$ ) at 697 K (424 °C) and cools to room temperature.<sup>[6]</sup> As indicated by a dashed vertical line in Figure 1, increasing the chromium content beyond 11.4 wt pct would result in bypassing the single-phase  $\gamma$  region and permit a certain amount of stable  $\delta$ -ferrite embedded in a martensitic matrix to be present at room temperature.

*In-situ* XRD experiments were performed at beamline 33-BM-C of the Advanced Photon Source at Argonne National Laboratory using a 30 keV X-ray beam. Test coupons measuring 100-mm long by 4.75-mm wide by 2-mm thick were heated at a rate of 10 Ks<sup>-1</sup> to a peak temperature ( $T_p$ ) of 1573 K (1300 °C), held for 3 seconds, and then cooled at the same rate to room temperature in an evacuated specimen chamber. Direct resistance heating was used to achieve the desired thermal cycle in the specimen. This temperature profile is similar to a thermal cycle experienced in the heat-affected zone adjacent to the weld fusion line. A schematic of the experimental setup is given in Figure 2. The heating rate was reduced in order to acquire sufficient diffraction patterns to be recorded during heating. Further details regarding the experimental setup are described elsewhere.<sup>[7]</sup>

The sample was scanned at 3-second intervals between  $d$ -spacing values of 1.1 to 2.3 Å, allowing three Debye arcs representing the austenite phase and three arcs representing the ferrite/martensite phase to be monitored. The Debye arcs were then converted into a 1-D plot showing intensity vs  $d$ -spacing. The amounts of

P. MAYR, Visiting Scientist, Department of Materials Science and Engineering, Massachusetts Institute of Technology, is on leave from the Institute for Materials Science and Welding, Graz University of Technology, 8010 Graz, Austria. Contact e-mail: peter.mayr@tugraz.at T.A. PALMER, Metallurgist, formerly with the Lawrence Livermore National Laboratory, is now Assistant Professor, with the Department of Materials Science and Engineering, Penn State University, University Park, PA 16802. J.W. ELMER, Group Leader for Materials Joining, is with the Lawrence Livermore National Laboratory, Livermore, CA 94550. E.D. SPECHT, Senior Research Staff Member, is with Oak Ridge National Laboratory, Oak Ridge, TN 37831. S.M. ALLEN, POSCO Professor of Physical Metallurgy, is with the Department of Materials Science and Engineering, Massachusetts Institute of Technology, Cambridge, MA 02139.

Manuscript submitted May 3, 2010.  
Article published online July 27, 2010

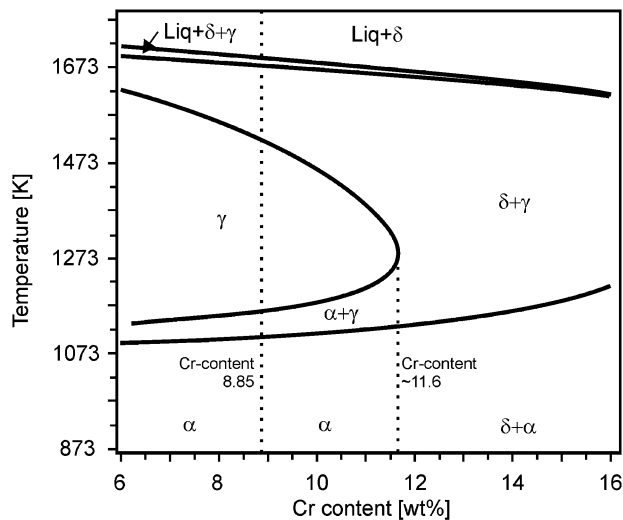


Fig. 1—Calculated isopleth for a martensitic steel with the chemical composition given previously but allowing the chromium content to range from 6 to 16 wt pct.

austenite and ferrite/martensite present at each time increment are then calculated using an analysis of the peaks present in each diffraction pattern and plotted as a function of time. A detailed description of the method is given elsewhere.<sup>[8]</sup> With this experimental setup, the X-rays do not penetrate very deeply so that mainly surface layers of martensite, austenite, and  $\delta$ -ferrite are studied. For validation of the XRD results and generation of additional specimens for further metallographic investigations, dilatometric experiments were performed using a Bähr DIL-805 A/D horizontal dilatometer (Bähr Thermoanalyse GmbH, Hüllhorst, Germany) and solid cylindrical specimens ( $4 \times 10$  mm).

Figures 3(a) through (c) summarize the sequence of observed phase transformations during the applied thermal cycle in a  $d$ -spacing vs time plot for the ferrite/martensite bcc-bct (110) and the austenite fcc (111) diffraction peaks and the calculated ferrite/martensite phase fractions. The difference in the lattice constants for the bcc and bct phases is very small, making it impossible to differentiate between ferrite and martensite using only the XRD results. It was therefore assumed that during cooling all of the bcc diffraction peaks represent the  $\delta$ -ferrite until the  $M_S$  temperature is reached. At this point, the amount of  $\delta$ -ferrite had decreased to 2 pct, and the increase of bcc/bct peaks as the temperature decreased below  $M_S$  was attributed solely to the formation of martensite.

Temperatures at which phase transformations occur were defined as where either 1 pct of a phase has formed ( $A_{C1}$ ,  $A_{C4}$ ,  $M_S$ ) or 99 pct of the transformation has been completed ( $A_{C3}$ ). Table I provides a summary of the calculated equilibrium temperatures for these selected transformation temperatures and compares them with the experimental results from the XRD and dilatometry experiments.

*In-situ* XRD shows that phase transformation of the tempered martensitic to a uniform austenitic structure occurs at temperatures between  $1153 \pm 15$  K

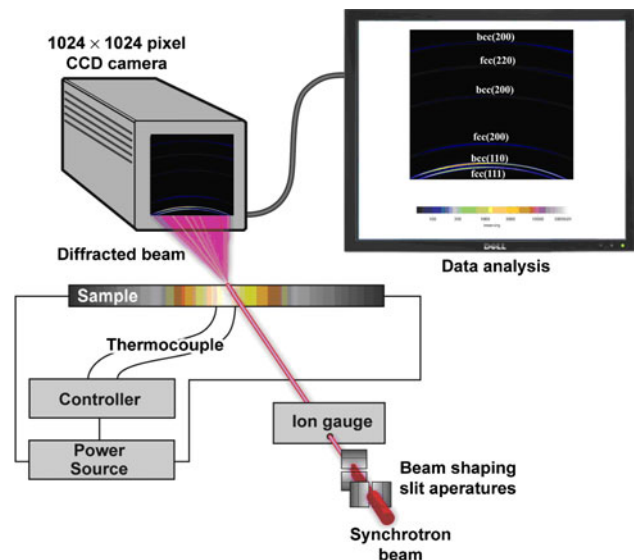


Fig. 2—Schematic of the experimental setup for the *in-situ* XRD experiments using synchrotron radiation during direct resistance heating of the specimen.

( $880 \pm 15$  °C) ( $A_{C1}$ ) and  $1305 \pm 15$  K ( $1032 \pm 15$  °C) ( $A_{C3}$ ). The uncertainty in measured transformation temperatures arises from the linear interpolation between two measured values at a 3-second interval ( $\Delta T = 30$  K). In the temperature range from  $1305 \pm 15$  K ( $1032 \pm 15$  °C) to  $1483 \pm 15$  K ( $1210 \pm 15$  °C), the steel exhibits a single-phase austenite lattice structure. At  $1483 \pm 15$  K ( $1210 \pm 15$  °C) ( $A_{C4}$ ), the formation of  $\delta$ -ferrite is initiated and a phase fraction of 19 pct is reached at a temperature of  $1573$  K ( $1300$  °C). On cooling,  $\delta$ -ferrite transforms back to austenite, but this transformation is incomplete and results in the retention of about 2 pct of  $\delta$ -ferrite before the martensitic transformation starts. The first formation of martensite is observed at  $676 \pm 5$  K ( $403 \pm 5$  °C) ( $M_S$ ). The level of uncertainty is reduced to  $\pm 5$  K due to a decrease in cooling rate ( $3$  s  $\sim \Delta T = 10$  K) in this region. When room temperature is reached, about 4 pct of austenite has not transformed to martensite and is retained.

Dilatometric measurements using a heating rate of  $10$  K s<sup>-1</sup> confirm the XRD results. In these measurements, the start of  $\delta$ -ferrite formation occurs at  $1553$  K ( $1260$  °C). Due to the lower sensitivity of dilatometric measurements, this temperature has a higher, but not quantifiable, degree of uncertainty. The presence of retained  $\delta$ -ferrite and austenite can also not be determined. Dilatometry showed  $A_{C1}$  temperature to be  $1165$  K ( $892$  °C),  $A_{C3}$   $1303$  K ( $1030$  °C),  $A_{C4}$   $1533$  K ( $1260$  °C), and  $M_S$  at  $713$  K ( $440$  °C). Measured values differ from the calculated equilibrium values due to the strong kinetic influence of heating and cooling rates on the phase transformations.

Optical micrographs (Figure 4) of the sample after thermal cycling revealed a martensitic microstructure with retained  $\delta$ -ferrite in two morphologies. The first is a skeletal morphology approximately 50- to 100- $\mu$ m wide and several hundred micrometers long. This skeletal  $\delta$ -ferrite has its origin in the formation of small stable

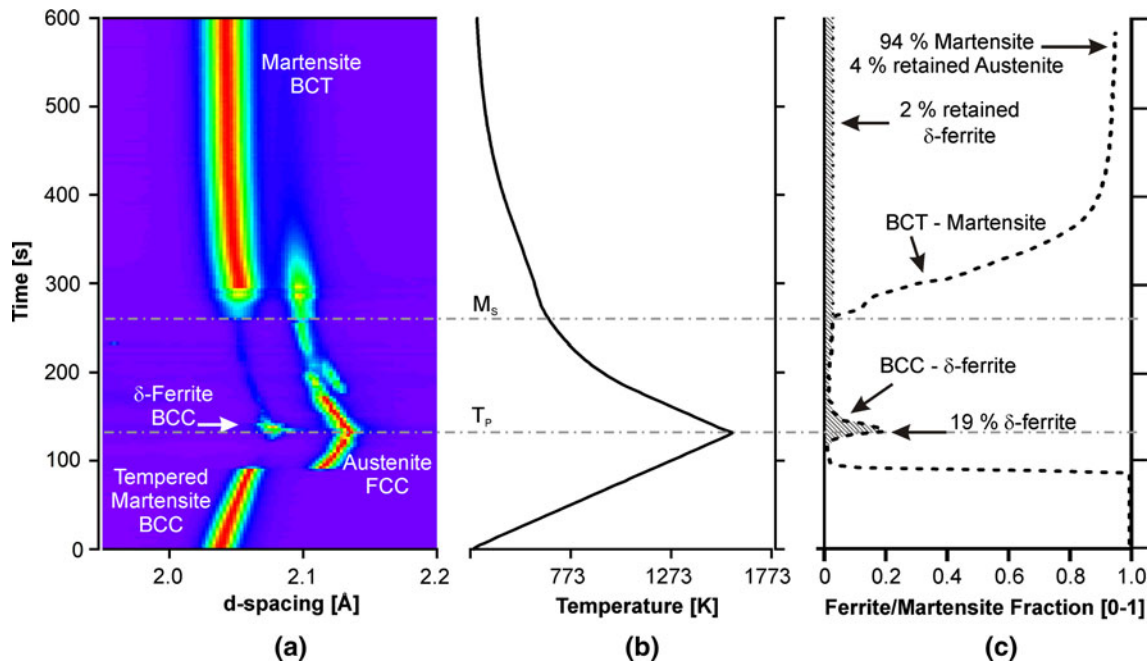


Fig. 3—Sequence of phase transformations shown by an intensity plot of the ferrite/martensite (110) and austenite (111) peaks (a) for a temperature cycle (b) characterized by heating to a peak temperature of 1573 K (1300 °C) with a rate of 10 Ks<sup>-1</sup> and subsequent cooling at the same rate. (c) Plot of the evolution of the ferrite-martensite (bcc/bct) phase fraction as a function of the thermal cycle.

**Table I. Comparison of Calculated Equilibrium and Measured Phase Transformation Temperatures during Thermal Cycling to a Peak Temperature of 1573 K (1300 °C) at 10 Ks<sup>-1</sup>**

	$A_{e1}/A_{c1}$	$A_{e3}/A_{c3}$	$A_{e4}/A_{c4}$	$M_S$
Equilibrium	1113 K (840 °C)	1168 K (895 °C)	1512 K (1239 °C)	*697 K (424 °C)
XRD	1153 ± 15 K (880 ± 15 °C)	1305 ± 15 K (1032 ± 15 °C)	1483 ± 15 K (1210 ± 15 °C)	676 ± 5 K (403 ± 5 °C)
Dilatometry	1165 K (892 °C)	1303 K (1030 °C)	1533 K (1260 °C)	713 K (440 °C)

\*Calculated for a driving force of 1400 J/mol.

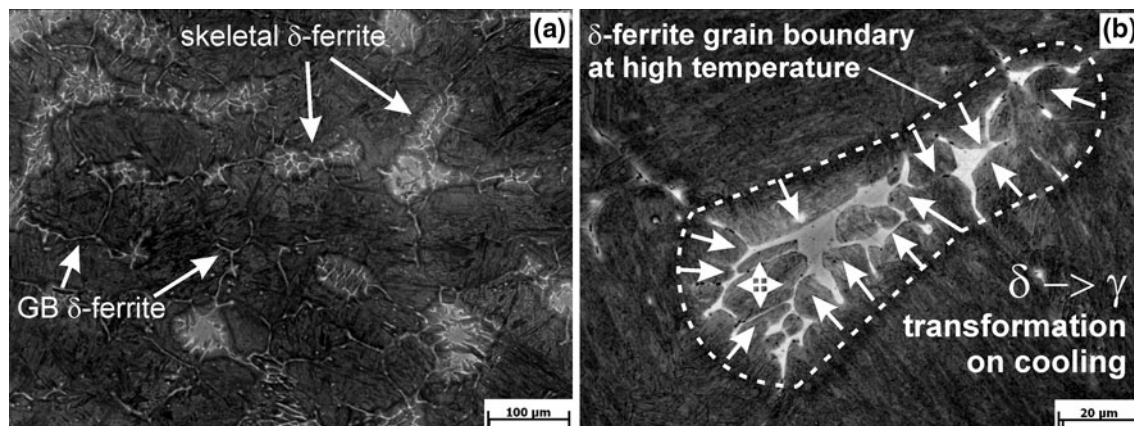


Fig. 4—(a) Optical micrograph of 9Cr steel after thermal cycling revealing martensitic matrix with skeletal and GB retained  $\delta$ -ferrite (bright phase) and (b) magnified section with the origin of the skeletal morphology delineated. The arrows in (b) indicate the direction of austenite formation during cooling.

homogeneous  $\delta$ -ferrite grains at or near the peak temperature. When reaching the  $A_{c4}$  temperature,  $\delta$ -ferrite nucleates at the austenite grain boundaries

and, with further heating, experiences a diffusion-governed growth, resulting in single equiaxed  $\delta$ -ferrite grains in the austenitic matrix.

On cooling,  $\delta$ -ferrite incompletely retransforms to austenite leaving a skeletal shaped network of retained  $\delta$ -ferrite. In this investigation, 17 pct of the  $\delta$ -ferrite present at its maximum retransformed to austenite on cooling, while 2 pct was retained. The skeletal morphology can be explained by preferred directions of the diffusion-governed  $\delta$ -ferrite to austenite transformation. Figure 4(b) shows, based on the etching response of the microstructure, the assumed  $\delta$ -ferrite grain boundary (GB) at high temperature, and arrows indicate the progression of the diffusion governed  $\delta$ -ferrite to austenite transformation leaving a skeletal shaped retained  $\delta$ -ferrite.

The second morphology of  $\delta$ -ferrite has a shell-like shape, only a few micrometers in width, surrounding prior austenite grains. These prior austenite grains with an average diameter of about 100  $\mu\text{m}$  are the result of the initial ferrite to austenite transformation on heating.  $\delta$ -ferrite formation starts at the prior austenite grain boundaries and proceeds faster in the direction of the GB compared to the grain interior due to enhanced diffusivity along the GB. On cooling, not all of the  $\delta$ -ferrite transforms back to austenite and a shell-like structure of retained  $\delta$ -ferrite surrounds the prior austenite grains.

The phase fraction of retained delta ferrite was evaluated by image analysis of optical micrographs using Zeiss KS400 Image Analysis Software (Carl Zeiss MicroImaging GmbH, Jena, Germany). To obtain statistically relevant values, a total area of  $6.3 \times 4.3 \text{ mm}$  was analyzed at a magnification of 200 times. Image analysis resulted in a measured mean  $\delta$ -ferrite fraction of 5.6 with a standard deviation of 1.9 pct. Since the phase fractions are measured based on color differences resulting from the different etching response of  $\delta$ -ferrite (bright) and martensite (dark), there is some uncertainty in the measurements. In particular, the skeletal regions of  $\delta$ -ferrite are surrounded by areas of martensite with lighter etching response comparable to the  $\delta$ -ferrite (Figure 4(b)) and, therefore, might be wrongfully added to the  $\delta$ -ferrite fraction. Retained austenite could not be identified in the micrographs since it is present as submicron sized laths (which fall below the resolution of optical microscopy) between martensite laths.

When compared to the equilibrium phase transformation temperatures, superheating on the order of 40 K to 50 K for the ferrite to austenite transformation is observed and attributed to the kinetic influence of the heating rate. On the contrary, the austenite to  $\delta$ -ferrite transformation in the XRD experiment started about 30 K below the calculated equilibrium value, which can be explained by local enrichment in chromium and molybdenum due to the dissolution of Cr-rich  $\text{M}_{23}\text{C}_6$  ( $T_{\text{sol}} = 1259 \text{ K}$  ( $986 \text{ }^\circ\text{C}$ )) along the prior austenite grain boundaries. Such segregated areas rich in ferrite-stabilizing elements are preferential points for  $\delta$ -ferrite nucleation.

The XRD measurements proved to be sensitive enough in detecting even a small volume fraction of  $\delta$ -ferrite and monitoring its evolution and retention. The data reveal that in the temperature range from  $1305 \pm 15 \text{ K}$  ( $1032 \pm 15 \text{ }^\circ\text{C}$ ) to  $1483 \pm 15 \text{ K}$  ( $1210 \pm 15 \text{ }^\circ\text{C}$ ), the steel exhibits a single-phase austenitic matrix. It is therefore possible that a fully martensitic matrix can be formed by annealing in this single-phase austenite temperature range followed by rapid cooling. A single-weld thermal cycle, characterized by an increased heating rate, low dwell time, and relatively fast cooling, inhibits the achievement of this equilibrium condition. More time in the austenitic single-phase region would be needed to compensate for the inhomogeneous elemental distribution caused by the dissolution of chromium carbides.

---

The support of PM through the Max Kade Foundation (New York) and the Austrian Academy of Sciences is gratefully acknowledged. This research was sponsored by the Division of Materials Sciences and Engineering, Office of Basic Energy Sciences, United States Department of Energy (EDS). Use of the Advanced Photon Source at Argonne National Laboratory was supported by the United States Department of Energy, Office of Science, Office of Basic Energy Sciences, under Contract No. DE-AC02-06CH11357.

**Open Access** This article is distributed under the terms of the Creative Commons Attribution Noncommercial License which permits any noncommercial use, distribution, and reproduction in any medium, provided the original author(s) and source are credited.

## REFERENCES

1. L. Schafer: *J. Nucl. Mater.*, 1998, vol. 263, pp. 1336–39.
2. *Creep Resistant Steels*, F. Abe, T.-U. Kern, and R. Viswanathan, eds., Woodhead Publishing Limited, Boca Raton, FL, 2008, pp. 279–304.
3. *Creep Resistant Steels*, F. Abe, T.-U. Kern, and R. Viswanathan, eds., Woodhead Publishing Limited, Boca Raton, FL, 2008, pp. 472–503.
4. *Mathematical Modelling of Weld Phenomena 5*, H. Cerjak and H.K.D.H. Bhadeshia, eds., IOM Communications, London, 2001, pp. 349–61.
5. “Thermodynamic Database ‘mc\_steel,’” Institute of Materials Science and Technology, Vienna University of Technology, Vienna, Austria, 2009.
6. J.C. Zhao and Z.P. Jin: *Acta Metall. Mater.*, 1990, vol. 38, pp. 425–31.
7. J.W. Elmer, T.A. Palmer, S.S. Babu, and E.D. Specht: *Mater. Sci. Eng. A-Struct.*, 2005, vol. 391, pp. 104–13.
8. J.W. Elmer, T.A. Palmer, W. Zhang, B. Wood, and T. DebRoy: *Acta Mater.*, 2003, vol. 51, pp. 3333–49.